JOM, Vol. 69, No. 1, 2017
DOI: 10.1007/s11837-016-2157-x

Elastic Property Dependence on Mobile and Trapped Hydrogen in Ni-201

S.K. LAWRENCE,[1,4,5] B.P. SOMERDAY,[2,3] and R.A. KARNESKY[1]

1.—Sandia National Laboratories, 7011 East Ave, Livermore, CA 94550, USA. 2.—Southwest Research Institute, 6220 Culebra Rd, San Antonio, TX 78238, USA. 3.—International Institute for Carbon-Neutral Energy Research (WPI-I2CNER), Kyushu University, 744 Moto-oka, Nishi-ku, Fukuoka 819-0395, Japan. 4.—*Present address:* Los Alamos National Laboratory, P.O. Box 1663, Los Alamos, NM 87545, USA. 5.—e-mail: slawrence@lanl.gov

Enhanced dislocation processes can accompany decohesion mechanisms during hydrogen degradation of ductile structural metals. However, hydrogen–deformation interactions and the role of defects in degradation processes remain poorly understood. In the current study, nanoindentation within specifically oriented grains in as-received, hydrogen-charged, aged, and hydrogen re-charged conditions revealed a "hysteresis" of indentation modulus, while the indentation hardness varied minimally. Thermal pre-charging with approximately 2000 appm hydrogen decreases the indentation modulus by ~20%, aging leads to a slight recovery, but re-charging drives the modulus back down to values similar to those measured in the hydrogen-charged condition. This "hysteresis" indicates that dissolved interstitial hydrogen is not solely responsible for mechanical property alterations; hydrogen trapped at defects also contributes to elastic property variation.

INTRODUCTION

Degradation of structural metals exposed to hydrogen has been linked to decreased ductility and fracture toughness. Extensive research has resulted in a number of proposed degradation mechanisms focusing on different aspects of hydrogen–material interactions, such as hydrogen absorption,[1] hydride formation,[2] plasticity effects,[3] and atomic bonding effects.[4] Of these, there are two widely accepted mechanisms attributed to hydrogen degradation in metals containing internal hydrogen that do not readily form hydrides. The hydrogen-enhanced localized plasticity (HELP) mechanism suggests that solute hydrogen atmospheres along the elastic strain field of a dislocation interact with those of neighboring dislocations, reducing the repulsive force between them and enhancing dislocation mobility.[3,5] In this way, hydrogen–dislocation interactions lead to localized plasticity in regions of high hydrogen concentration and ultimately cause macroscopic brittle fracture via locally ductile processes.[3,5]

In contrast, observations of low-ductility fracture, occurring without significant plasticity in hydrogen-exposed non-hydride-forming systems[4,6,7] led to the establishment of the hydrogen-enhanced decohesion (HEDE) mechanism. HEDE assumes that dissolved hydrogen weakens interatomic bonds at grain boundaries or other interfaces, and therefore lowers the cohesive energy, resulting in brittle failure at low applied stresses[6,7] and increased intergranular fracture in some systems.[8,9]

Additionally, recent investigations, such as those by Nagumo,[10] point to the importance of vacancies in degradation processes. The hydrogen-enhanced strain-induced vacancy (HESIV) theory suggests that hydrogen enhances vacancy formation and agglomeration during deformation.

The objective of the current study is to assess the impact of dissolved hydrogen on mechanical properties, measured in small material volumes, to ascertain the dominant degradation mechanism. Commercially pure Ni-201 has been chosen for this investigation because it is a model system for structural materials such as nickel-based superalloys and austenitic stainless steels, and is susceptible to hydrogen-induced intergranular fracture. Given these material attributes, the principal degradation mechanism can be identified based on material response to hydrogen charging and

(Published online November 21, 2016)

deformation. For example, if HELP dominates, hardness would likely vary, due to enhanced dislocation motion during plasticity, but dislocation cross-slip would be restricted.[11,12] Conversely, if HEDE dominates, an overall decrease in bulk modulus (which is related to the cohesive energy) may be observed. Nanoindentation is an ideal method to probe orientation-dependent material response in the presence of hydrogen because it enables statistical analysis of properties measured with high fidelity in a small sampled area, and it has been used to investigate small-volume material behavior in a variety of hydrogenated face centered cubic (FCC) alloys.[13–15] Here, mechanical properties are measured with nanoindentation; elastic modulus (related to bulk modulus by Poisson's ratio) and hardness are compared as a function of crystallographic orientation and hydrogen concentration.

EXPERIMENTAL

Nanoindentation experiments were conducted on Ni-201, a commercially pure nickel alloy, supplied by ATI Allegheny Ludlum. The only impurities above 10 wt ppm, as measured by glow discharge mass spectroscopy and instrumental gas analysis, are (in wt ppm): 630 Al, 550 Si, 130 C, 44 Fe, and 27 Mg. The S concentration, which segregates to Ni grain boundaries and enhances degradation,[9] is particularly low (0.54 wt ppm). The as-received Ni-201 plate was annealed at 1173 K for 1 h, resulting in a mean grain size of 1 mm. Specimens were prepared by standard metallographic procedures, concluding with a polish using 0.05-μm colloidal silica suspension. Electron backscatter diffraction (EBSD) orientation imaging was employed to determine grain orientations. Grains with near-(001), (101), and (111) orientations, as well as three grains with intermediate orientations, were identified for indentation; the three indented grains are labeled with approximate orientations in Fig. 1. Nanoindentation measurements to determine mechanical properties were performed using a Nanoindenter XP equipped with a nominally 150-nm-radius Berkovich probe. The same grains were indented in all four conditions so that no large-scale orientation variations affected the measurements. Stiffness, modulus, and hardness values were obtained through dynamic indentation using the continuous stiffness module (CSM) at a frequency target of 20 Hz, displacement target of 1 nm, and a 1500-nm-depth limit. Indents were arranged in 7 × 7 arrays (49 indents), spaced 25 μm apart, ensuring no indent was affected by the plastic zone of a previous indent. All arrays were located well within the grain interior, but separated from each other by at least 100 μm.

Atomic hydrogen was dissolved into the Ni-201 specimens by thermally charging in high-pressure hydrogen gas following a standard procedure described elsewhere.[12,16] Charging was conducted at elevated temperature to enhance hydrogen diffusion, but temperatures were limited to avoid thermally-activated microstructural changes in the nickel. Samples were charged at a hydrogen gas pressure of 82 MPa and temperature of 473 K for 280 h to achieve a hydrogen concentration of ~2000 appm. Indentation was performed, following the method described previously, in the same grains as were indented in the as-received condition.

The samples were then aged at room temperature for approximately 1 year and the same grains were indented following the aforementioned procedure. The diffusivity of hydrogen in Ni at room temperature is $D_H \sim 10^{-10}$ cm^2 s^{-1} (a root-mean-square diffusion distance, $\sqrt{4Dt}$, of 3 mm) while the solubility is only ~7 appm MPa$^{-1/2}$[17] thus hydrogen in lattice interstitial sites would be expected to egress from the samples during the aging time. Conversely, hydrogen bound to trap sites, such as dislocations or vacancies, would be retained in the microstructure because trap sites are both abundant[17,18] and effectively immobile at ambient temperature. For instance, vacancy diffusivity, $D_v \sim 10^{-20}$ cm^2 s^{-1} ($\sqrt{4Dt}$ = 1 μm),[19] multiple orders of magnitude smaller than D_H. Finally, the samples were re-charged with hydrogen, at a pressure of 62 MPa, temperature of 573 K, for 144 h, inducing a concentration of ~3000 appm. Nanoindentation was conducted in the re-charged condition, following the above-mentioned procedure.

Hydrogen thermal desorption spectra (TDS) were obtained in the temperature range 300–1000 K at a constant heating rate of 6 K min^{-1} by measuring the hydrogen partial pressure in the vacuum chamber of a TDS apparatus. The base pressure in the apparatus was kept better than 10^{-4} Pa.

RESULTS AND DISCUSSION

Hydrogen Content and Trapping

The bulk hydrogen concentration in the hydrogen-charged samples was ~2000 and ~3300 appm in the re-charged samples, as measured by inert gas fusion analysis (IMR Test Labs, Portland, OR). Analysis of a similar sample charged with ~2000 appm H and then aged for 2 years at room temperature detected a hydrogen concentration of ~1000 appm. Hydrogen occupies octahedral interstitial sites in the Ni lattice as well as trap sites, such as vacancies, dislocation cores, or grain boundaries. The measured decrease is likely associated with hydrogen egress from interstitial sites, which typically have lower binding energies for hydrogen.[17] In fact, TDS analysis of a Ni-201 sample precharged with 4000 appm hydrogen and then aged for 2 years indicates both a reduction in the total hydrogen content to approximately 2000 appm and a prominent peak at 700 K (Fig. 2), corresponding to hydrogen bound at trap sites.[20] Based on these

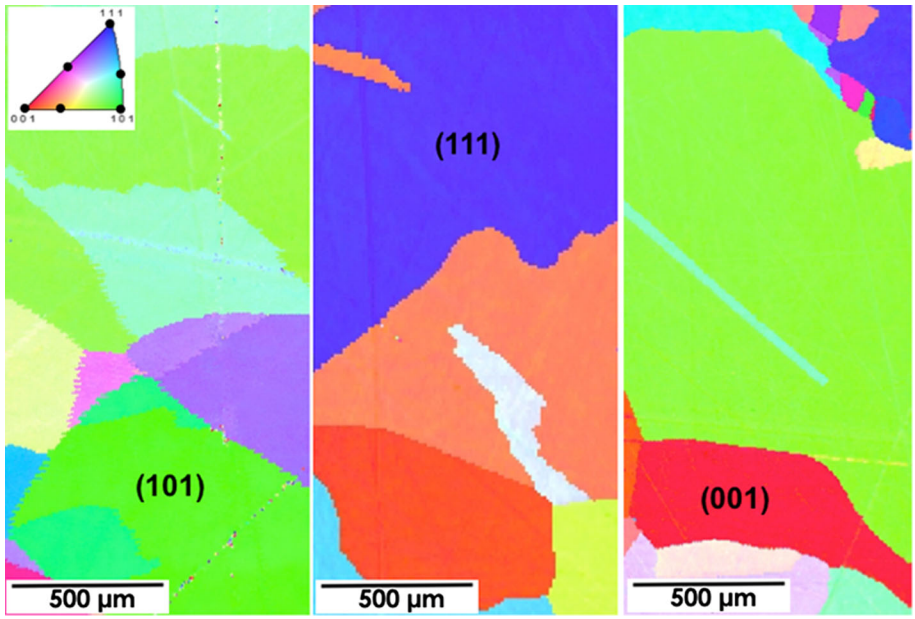

Fig. 1. Inverse pole figure maps indicating grain orientations. Three grains selected for indentation are labeled with their approximated orientations. All grain locations are marked on the inset stereographic triangle.

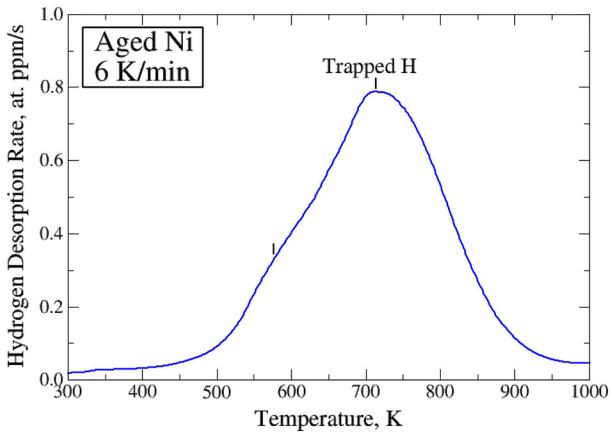

Fig. 2. Thermal desorption spectra of Ni-201 pre-charged with ~4000 appm hydrogen then aged at room temperature for approximately 2 years, yielding ~2000 appm hydrogen. The peak marked at ca. 700 K indicates that most of the remaining hydrogen is trapped.

data, we estimate that the aged samples contained at least 1000 appm hydrogen, primarily trapped, rather than interstitial.

Mechanical Properties

Examples of nanoindentation load–displacement curves for the as-received, hydrogen-charged, aged, and re-charged conditions are shown in Fig. 3. Variation in indentation modulus can be identified by the dissimilarity in unloading slopes of the four curves. Table I summarizes the average elastic modulus and hardness for each material condition; only values collected for indent depths greater than 200 nm were analyzed to ensure depth-independence, as described in Supplement 1. The modulus values measured for the as-received ⟨001⟩, ⟨101⟩, and ⟨111⟩ grains are highly anisotropic and similar to accepted literature values.[21] The values for the intermediate orientations fall within a reasonable range given their respective bounding orientations and anisotropy effects. Note that traditional indentation contact mechanics analyses were developed for isotropic materials, but Vlassak and Nix[22] have shown that the indentation modulus can be calculated for arbitrary anisotropic solids. Their formulae are employed here to derive theoretical indentation moduli, M, for the three primary grain orientations:

$$M = 1.058\beta_{\mathrm{hkl}}\left(\frac{E}{1-\nu^2}\right)_{\mathrm{isotropic}}, \qquad (1)$$

where the pre-factor 1.058 is a stiffness adjustment for tips with a triangular geometry, E is the elastic modulus, ν is Poisson's ratio, and β_{hkl} is a correction factor calculated by:

$$\beta_{\mathrm{hkl}} = a + c(A - A_{\mathrm{o}})^{\mathrm{B}}. \qquad (2)$$

In Eq. 2, A is the anisotropy factor, and a, c, B, are constants determined from Poisson's ratio in the cube directions. M has been calculated for each of the cube directions in Ni using tabulated values for elastic modulus[21] (Table I). Measured elastic modulus values in the as-received condition differ from these calculated values by only 5%, indicating that comparing measured modulus values will provide an accurate assessment of elastic property changes as a function of hydrogen charging. Note that some variability in measured indentation modulus within a grain is expected due to minute real and apparent orientation gradients (e.g., caused by fluctuating surface quality and near-surface defect densities).

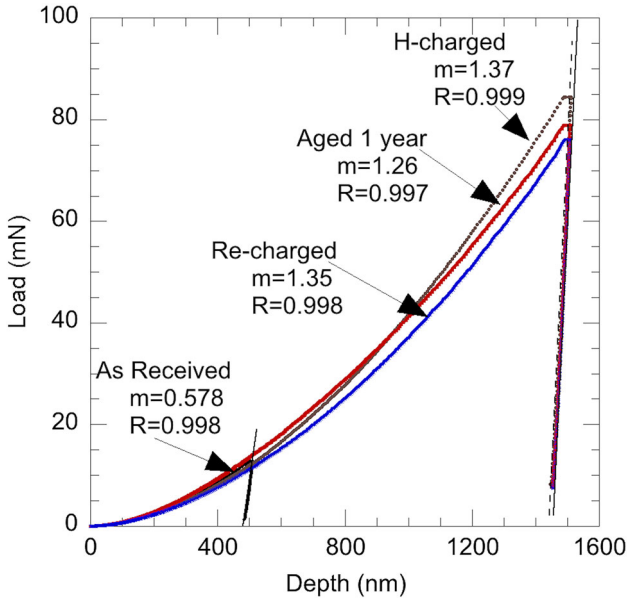

Fig. 3. Representative indentation load-depth curves reveal variation in unloading slope with hydrogen content, suggesting hydrogen alters elastic properties. Conversely, the similarity in initial loading slopes indicates minimal hardness variation with hydrogen content.

Upon pre-charging with hydrogen, the indentation modulus in all six grain orientations decreases approximately 22%, while indentation hardness varies minimally (Table I). Indentation modulus partially recovers after aging at room temperature for approximately 1 year (Table I); the values increase by ~8% as compared to the hydrogen-charged moduli. However, the aged modulus values are still ~11% lower than the as-received moduli. Exposing the samples to a second thermal hydrogen-charging cycle drives the indentation modulus back down to values comparable with those measured after initial charging (~20% lower than as-received moduli).

While interstitial hydrogen contributes to the elastic property variation, partial recovery with aging indicates that it is not solely responsible. Rather, hydrogen trapped at defects, including hydrogen-induced defects, may drive the measured reduction in elastic modulus in the aged condition. Vacancy clusters are one such defect that can form during hydrogen charging and readily trap hydrogen. Positron annihilation spectroscopy investigations suggest that high pressure (5 GPa), high temperature (1123 K) hydrogen charging enhances formation of non-equilibrium "superabundant vacancies"[23,24] and that hydrogen stabilizes strain-induced vacancies.[10,25,26] While the hydrogen charging conditions applied during this investigation are modest in comparison, it is likely that thermally-induced vacancy formation is encouraged during the elevated-temperature charging cycle; Carr and McLellan[27] calculated the vacancy concentration in hydrogen-charged Ni at 573 K to be about 21 times greater than that of pure Ni. Importantly, it is energetically favorable for vacancies to agglomerate and form V_xH_n vacancy–hydrogen complexes,[28] which can alter local electronic or atomic structure, thereby changing the elastic properties measured during indentation of a material volume containing such complexes.

The substantial modulus reduction detected after hydrogen charging (~22%) is similar in magnitude to the 21% decrease in indentation modulus measured by Nibur et al.,[29] after thermally charging 21Cr-6Ni-9Mn stainless steel. Similarly, Barnoush and Vehoff[13] reported a 28% decrease in the shear modulus of Ni that was cathodically charged in situ and indented. The authors of the latter paper attribute the decrease to a hydrogen-induced cohesive energy reduction. Other published data have detected smaller hydrogen-induced reductions in elastic modulus[30,31] and shear modulus.[31]

In contrast, hardness variation with orientation and testing condition is subtler. Based on an empirical cumulative distribution analysis, a clear hydrogen-induced hardness change is only discernible in the ⟨111⟩ grain. In this case, hardness values for the charged, aged, and re-charged conditions differ by only ~4%, but they are approximately 20% lower than the as-received hardness. A slight decrease is detected between the hydrogen-affected conditions and the as-received condition for the ⟨101⟩ grain (though the trend is obscured by data variability), but no such change is observed for the ⟨001⟩ grain. In light of this, the hardness decrease may be the combined result of both recovery of the near-surface damage layer induced by sample preparation and plastic accommodation. The effect likely appears most pronounced in the ⟨111⟩ grain due to the availability of multiple active slip systems along which dislocations may move. In a previous study,[12] the authors found that hardness measured by quasistatic nanoindentation was also insensitive to hydrogen concentration. Hydrogen charging extended the plastic zone formed around each indent and increased the spacing between slip steps, as a result of cross-slip restriction; the authors proposed that a larger plastic zone accommodated the enhanced dislocation motion suggested by the HELP theory. While the plastic zone length was not measured directly during the current study, it is probable that a similar dislocation accommodation occurs in this case, limiting hardness variation with hydrogen content.

SUMMARY

Dynamic nanoindentation was used to assess hydrogen effects on mechanical properties in Ni-201. Notably, a hysteresis in measured indentation modulus is observed when Ni is first hydrogen-charged, then aged at room temperature, which depletes interstitial hydrogen, and re-charged once more. Hydrogen charging reduces the indentation

Table I. Hardness and elastic modulus as a function of hydrogen charging condition and crystallographic orientation; theoretical indentation modulus, *M*, is included for comparison with measured as-received values, and values are averaged for more than 35 indents per grain

Orientation	Th. modulus (GPa) Calculated	Modulus (GPa)				Hardness (GPa)			
		As received	H-charged	RT aged	Re-charged	As received	H-charged	RT aged	Re-charged
001	194	191 ± 18	157 ± 11	171 ± 16	145 ± 10	1.8 ± 0.3	1.7 ± 0.1	1.8 ± 0.2	1.6 ± 0.1
110	215	204 ± 20	167 ± 17	182 ± 15	157 ± 10	2.2 ± 0.3	1.9 ± 0.1	1.9 ± 0.1	1.7 ± 0.1
111	222	218 ± 11	180 ± 20	190 ± 17	185 ± 22	2.3 ± 0.2	1.8 ± 0.3	1.8 ± 0.2	1.8 ± 0.2
001–111		221 ± 17	179 ± 19			2.7 ± 0.5	2.1 ± 0.3		
001–110		228 ± 16	177 ± 21			2.6 ± 0.2	1.9 ± 0.3		
110–111		218 ± 21	189 ± 18			2.5 ± 0.4	2.1 ± 0.2		

modulus by ~20%, aging at room temperature leads to limited recovery, but re-charging drives the modulus back down to values commensurate with the initial hydrogen-charged condition. This effect is linked to the significant trapped hydrogen content retained in the microstructure even after long-term room-temperature aging, despite the depletion of interstitial hydrogen. Thus, both interstitial hydrogen (when present) and hydrogen trapped in the defect structure induced by hydrogen-charging (present even when interstitial hydrogen is depleted) likely change the local structure, leading to a measureable change in elastic properties as a function of hydrogen concentration.

ACKNOWLEDGEMENTS

This work was supported by the DOE NNSA Stewardship Science Graduate Fellowship [Grant DE-NA0002135] (SKL) and the Laboratory Directed Research and Development program at Sandia National Laboratories [Grant SNL-LDRD-173116], a multi-mission laboratory managed and operated by Sandia Corporation, a wholly owned subsidiary of Lockheed Martin Corporation, for the U.S. Department of Energy's National Nuclear Security Administration under Contract DE-AC04-94AL85000.

ELECTRONIC SUPPLEMENTARY MATERIAL

The online version of this article (doi:10.1007/s11837-016-2157-x) contains supplementary material, which is available to authorized users.

REFERENCES

1. S.P. Lynch, *Corros. Sci.* 22, 925 (1982).
2. W. Gerberich, *Gaseous Hydrogen Embrittlement of Materials in Energy Technologies Volume 2: Mechanisms, modeling and future developments*, ed. R.P. Gangloff and B.P. Somerday (Philadelphia: Woodhead, 2012), pp. 209–246.
3. H.K. Birnbaum and P. Sofronis, *Mater. Sci. Eng. A* 176, 191 (1994).
4. R. Oriani and P. Joshephic, *Acta Metall.* 22, 1065 (1974).
5. Y. Jagodzinski, H. Hanninen, O. Tarasenko, and S. Smuk, *Scr. Mater.* 43, 245 (2000).
6. J. Kameda and C. McMahon, *Metall. Mater. Trans. A* 11, 91 (1980).
7. W.W. Gerberich and Y.T. Chen, *Metall. Trans. A* 6, 271 (1975).
8. R.H. Jones, S.M. Bruemmer, M.T. Thomas, and D.R. Baer, *Metall. Mater. Trans. A* 14, 1729 (1983).
9. S.M. Bruemmer, R.H. Jones, M.T. Thomas, and D.R. Baer, *Metall. Mater. Trans. A* 14, 223 (1983).
10. M. Nagumo, *Mater. Sci. Technol.* 20, 940 (2004).
11. D. Delafosse, *Gaseous Hydrogen Embrittlement of Materials in Energy Technologies Volume 2: Mechanisms, modeling and future developments*, ed. R.P. Gangloff and B.P. Somerday (Philadelphia: Woodhead, 2012), pp. 247–285.
12. S.K. Lawrence, B.P. Somerday, N.R. Moody, and D.F. Bahr, *JOM J. Miner. Met. Mater. Soc.* 66, 1383 (2014).
13. A. Barnoush and H. Vehoff, *Scr. Mater.* 55, 195 (2006).
14. A. Barnoush and H. Vehoff, *Acta Mater.* 58, 5274 (2010).

15. N. Kheradmand, J. Dake, and A. Barnoush, *Philos. Mag.* 92, 3216 (2012).
16. S. Bechtle, M. Kumar, B.P. Somerday, M.E. Launey, and R.O. Ritchie, *Acta Mater.* 57, 4148 (2009).
17. M.R. Louthan Jr., J.A. Donovan, and G.R. Caskey Jr., *Acta Metall.* 23, 745 (1975).
18. A. Metsue, A. Oudriss, and X. Feaugas, *J. Alloys Compd.* 656, 555 (2016).
19. Y. Wang, D. Connétable, and D. Tanguy, *Phys. Rev. B* 91, 1 (2015).
20. O. Todoshchenko, Y. Yagodzinskyy, and H. Hänninen, *Defect Diffus Forum* 344, 71 (2013).
21. W. Betteridge, *Nickel and Its Alloys* (West Sussex: Ellis Horwood Ltd, 1984).
22. J.J. Vlassak and W.D. Nix, *J. Mech. Phys. Solids* 42, 1223 (1994).
23. Y. Fukai and N. Okuma, *Phys. Rev. Lett.* 73, 1640 (1994).
24. H. Osono, T. Kino, Y. Kurokawa, and Y. Fukai, *J. Alloys Compd.* 231, 41 (1995).
25. K. Takai, H. Shoda, H. Suzuki, and M. Nagumo, *Acta Mater.* 56, 5158 (2008).
26. M. Hatano, M. Fujinami, K. Arai, H. Fujii, and M. Nagumo, *Acta Mater.* 67, 342 (2014).
27. N. Carr and R. Mclellan, *J. Phys. Chem. Solids* 67, 1797 (2006).
28. D. Tanguy, Y. Wang, and D. Connétable, *Acta Mater.* 78, 135 (2014).
29. K. Nibur, D. Bahr, and B. Somerday, *Acta Mater.* 54, 2677 (2006).
30. F.M. Mazzolai and H.K. Birnbaum, *J. Phys. F Met. Phys.* 15, 525 (1985).
31. E. Lunarska, A. Zielnski, and M. Smialowski, *Acta Metall.* 25, 305 (1977).